Biochimica et Biophysica Acta 1828 (2013) 2729–2738

Contents lists available at ScienceDirect

Biochimica et Biophysica Acta

journal homepage: www.elsevier.com/locate/bbamem

Molecular mechanism of Ca^{2+}-catalyzed fusion of phospholipid micelles

Hui-Hsu Gavin Tsai *, Wei-Fu Juang, Che-Ming Chang, Tsai-Yi Hou, Jian-Bin Lee

Department of Chemistry, National Central University, Jhong-Li City, Tao-Yuan County 32001, Taiwan

ARTICLE INFO

Article history:
Received 24 January 2013
Received in revised form 14 July 2013
Accepted 17 July 2013
Available online 2 August 2013

Keywords:
Membrane fusion
Ca2 + -lipid cluster
Pre-stalk state
Stalk state
Free energy landscape
Fusion mechanism

ABSTRACT

Although membrane fusion plays key roles in intracellular trafficking, neurotransmitter release, and viral infection, its underlying molecular mechanism and its energy landscape are not well understood. In this study, we employed all-atom molecular dynamics simulations to investigate the fusion mechanism, catalyzed by Ca^{2+} ions, of two highly hydrated 1-palmitoyl-2-oleoyl-*sn*-3-phosphoethanolamine (POPE) micelles. This simulation system mimics the small contact zone between two large vesicles at which the fusion is initiated. Our simulations revealed that Ca^{2+} ions are capable of catalyzing the fusion of POPE micelles; in contrast, we did not observe close contact of the two micelles in the presence of only Na^{+} or Mg^{2+} ions. Determining the free energy landscape of fusion allowed us to characterize the underlying molecular mechanism. The Ca^{2+} ions play a key role in catalyzing the micelle fusion in three aspects: creating a more-hydrophobic surface on the micelles, binding two micelles together, and enhancing the formation of the pre-stalk state. In contrast, Na^{+} or Mg^{2+} ions have relatively limited effects. Effective fusion proceeds through sequential formation of pre-stalk, stalk, hemifused-like, and fused states. The pre-stalk state is the state featuring lipid tails exposed to the inter-micellar space; its formation is the rate-limiting step. The stalk state is the state where a localized hydrophobic core is formed connecting two micelles; its formation occurs in conjunction with water expulsion from the inter-micellar space. This study provides insight into the molecular mechanism of fusion from the points of view of energetics, structure, and dynamics.

1. Introduction

Membrane fusion plays a significant biological role in, for example, intracellular trafficking, recycling, viral inflecting, and neurotransmitter release. Its medical applications include drug delivery and gene therapy. Membrane fusion can occur through two reaction pathways: direct fusion and indirect fusion [1]. The differences between these two pathways are that the latter uniquely involves the formation of a stalk state and a hemifusion diaphragm. Membrane fusion is a complex physiological process regulated by fusion proteins, including soluble *N*-ethylmaleimide–sensitive factor attachment protein receptors (SNAREs), synaptotagmin, and others that bind to selected membranes at the same time, bringing them within a close distance to facilitate fusion through the direct fusion pathway [2]. The subsequent fusion stages are considered to be dependent mainly on the physical properties of the lipid membranes. In addition to fusion proteins, several other factors can induce membrane fusion, including the membrane tension [3], the temperature, the lipid composition of the membrane [4], and cation binding [5].

Although membrane fusion can be catalyzed by various factors, they all share a common mechanism. According to the stalk hypothesis on protein-free and pure lipid membranes, membrane fusion proceeds through at least five sequential steps: the approach of two membranes at a short distance; contact of two proximal monolayers with local perturbation; formation of a stalk state; formation of a hemifused state; and, finally, opening of a fusion pore [1,6]. The relative energies of these states and the energy barriers separating these two consecutive states depend on the hydration levels, the lipid compositions, and the catalysts. The stalk state comprises multiple lipid molecules bridging two apposed lipid monolayers. This stalk state expands to form a hemifused state that features a hemifused diaphragm between two distal leaflets.

Many efforts have been made to determine the structures of the fusion intermediates. Stalk states have been observed directly using X-ray diffraction [7,8], revealing that they are thermodynamically stable under certain conditions. A molecular dynamics (MD) simulation using a coarse-grained (CG) potential has also suggested the existence of a stable stalk or stalk-like state [9–11]. In quests to determine the rate-limiting steps of the fusion processes, many studies have focused on estimating the relative free energies of the fusion intermediates. MD simulations of the solvent molecules using CG models with different levels of complexity have yielded diverse free energies for the stalk state—from $6k_BT$ in small 1-palmitoyl-2-oleoyl-*sn*-3-phosphoethanolamine (POPE) vesicles [11] to $15k_BT$ in planar bilayers [12]. Continuum models [13,14] have provided estimates of the free energy for the stalk state that have varied from 25 to $50k_BT$—values higher than those estimated using CG models. A dissipative particle dynamics simulation suggested that the formation of a splayed lipid bond state is the critical step for lipid mixing of two bilayers under tension [15]. Recent related MD simulations using a CG model suggested that a pre-stalk state featuring

* Corresponding author. Tel.: +886 3 4227151x65909; fax: +886 3 4227664.
E-mail address: hhtsai@cc.ncu.edu.tw (H.-H.G. Tsai).

0005-2736/$ – see front matter © 2013 Elsevier B.V. All rights reserved.
http://dx.doi.org/10.1016/j.bbamem.2013.07.022

solvent-exposed tails is the transition state for membrane fusion [14,16].

Calcium (Ca^{2+}) ions play an important role in triggering synaptic vesicle fusion, which allows the transmitter to be released at neuronal synapses. In these processes, Ca^{2+} ions rapidly build up to become highly localized around the open Ca^{2+} ion channels near the presynaptic active zones. Surprisingly, a low concentration (10–25 M) of local Ca^{2+} ions is sufficient to ensure the release of the physiological transmitter [17]. The Ca^{2+} ion-triggered vesicle fusion at large central nervous system (CNS) synapses is highly cooperative, requiring four or five Ca^{2+} ions. Moreover, the fusion time is brief—less than 1 ms. Such fast kinetics suggests that the Ca^{2+} ions do not induce transmitter release through a complex mechanism [2].

Early in vitro experiments revealed that fusion occurs between phospholipid vesicles in the presence of Ca^{2+} ions [5,18]. Many subsequent studies using a variety of experimental techniques [5,19–22] and computational simulations [23,24] have demonstrated that Ca^{2+} ions interact strongly with lipid head groups. Calcium ions also interact strongly with anionic lipids to induce anionic phosphatidylserine (PS) domains in zwitterionic phosphocholine (PC) bilayers [25–28]—a process that has been implicated as an important step in membrane fusion. Moreover, they also interact strongly with zwitterionic PC lipids [21,29], Recently, we used all-atom MD simulations to demonstrate that Ca^{2+} ions can form complexes with phospholipids and that these complexes further assemble to form various multiple-cation–centered clusters in the presence of anionic lipids and at high ionic strength; in contrast, Na^{+}, K^{+}, and divalent Mg^{2+} ions exhibit limited capacity [24]. Potoff and co-workers used all-atom MD simulations to determine that Ca^{2+} ions can form anhydrous complexes with phospholipids between apposed bilayers [23].

Although there have been many comprehensive studies aimed at understanding common membrane fusion mechanisms [1,2], the underlying molecular processes and their energy landscapes remain poorly understood. In this study, we employed all-atom MD to simulate the fusion of two POPE micelles at high hydration in the presence of Ca^{2+}, Na^{+}, or Mg^{2+} ions. We observed that Ca^{2+} ions play a key role in catalyzing the fusion. We determined the free energy landscape of fusion catalyzed by Ca^{2+} ions and then characterized the underlying mechanism of the fusion process at the molecular level.

2. Methods

To capture the essential features of biomembrane fusion—in particular, those catalyzed by Ca^{2+} ions—all-atom MD was used to simulate the fusion of two POPE micelles in a spontaneous manner. Previous studies of membrane fusion using lipid bilayer models have been limited to investigations of early stage fusion [14,23], mainly because the water molecules between two fused leaflets could not be expelled in those simulations, due to the setup of the periodic boundary conditions (PBC), thereby retarding further fusion. On the other hand, although simulations using vesicle models are more-realistic mimics of biomembrane environments, their large size usually requires reduced CG models [30]; although they speed up the calculations, these CG models are sometimes too simple to present specific interactions in detail, including cation–lipid, water–water, and water–lipid interactions. To balance the advantages and disadvantages of the commonly used models, in this study a micelle model was employed that was smaller than the vesicle model, thereby allowing the roles of water molecules and Ca^{2+} ions during fusion to be studied using a full-atom force field. Although micelles are smaller than vesicles, this simulation system mimics the small contact zone between two large vesicles at which fusion is initiated.

Simulations of a single POPE micelle were first performed to obtain the stable micelle structure. The chemical structure of zwitterionic POPE is presented in the Supporting Information (SI, Fig. S1). The micelle comprised 62 POPE lipids. To prepare the micelle structure prior to simulation, the 62 POPE lipids were arranged spherically with the hydrophobic tails pointing inward. This initial structure contained large voids; after 0.8-ns MD simulation in vacuum at 300 K, however, the initial structure shrank into a compact micelle having a hydrophobic core. Thereafter, this compact micelle was solvated with water molecules and ions. Three simulations were performed using 0.15 M NaCl, $MgCl_2$, and $CaCl_2$, herein denoted as POPE-Na^{+}, POPE-Mg^{2+}, and POPE-Ca^{2+}, respectively. The minimum distance from the micelle to the box boundary was approximately 10 Å; the water-to-lipid ratio was approximately 180, providing a lipid concentration of approximately 0.31 M, which is much higher than the critical micelle concentration (ca. 0.001 M).

Three systems containing two micelles were examined: one containing 0.15 M NaCl (denoted 2 M-POPE-Na^{+}), one containing 0.15 M $MgCl_2$ (denoted 2 M-POPE-Mg^{2+}), and one containing 0.15 M $CaCl_2$ (denoted 2 M-POPE-Ca^{2+}). These two-micelle systems were constructed from the equilibrated structures of the single-micelle systems. The two micelles were arranged with a minimum distance of approximately 6 Å between the atoms of the two micelles. The minimum distance from a micelle to the box boundary was approximately 10 Å. To obtain better statistical results, the 2 M-POPE-Ca^{2+} system was simulated four times with different initial configurations, denoted 2 M-POPE-Ca^{2+}-SysI, 2 M-POPE-Ca^{2+}-SysII, 2 M-POPE-Ca^{2+}-SysIII, and 2 M-POPE-Ca^{2+}-SysIV; the 2 M-POPE-Na^{+} system was simulated twice with different initial configurations, denoted 2 M-POPE-Na^{+}-SysI and 2 M-POPE-Na^{+}-SysII; and the 2 M-POPE-Mg^{2+} system was simulated twice with different initial configurations, denoted 2 M-POPE-Mg^{2+}-SysI and 2 M-POPE-Mg^{2+}-SysII; the different initial configurations were created by rotating and separating the micelles in a random manner. The water-to-lipid ratio was approximately 191 for the two-micelle systems. Table 1 summarizes the setups of the simulation systems.

The lipids and counter ions were modeled using the CHARMM36 [31] all-atom force field; the water molecules were modeled using the TIP3 model [32]. All MD simulations were performed using parallel MD NAMD 2.7b3 software [33] with an NPT ensemble under three-dimensional periodic boundary conditions. The simulation temperature was controlled to physiological temperature (310 K) by Langevin dynamics; the pressure was controlled to 1 bar using the Langevin piston Nosé–Hoover method [34]; the three orthogonal dimensions of the periodic cell were allowed to change independently. Cutoffs of 12.0 and 13.5 Å were applied to calculate the pairwise interactions and to generate the neighboring list of pairs, respectively. The non-bonded neighboring list was updated every 10 steps. The particle-mesh Ewald technique was used to treat the long-range electrostatic interactions. The default Lennard-Jones (LJ) parameters for the cation–anion pair interaction obtained from the Lorentz–Berthelot combining rule were used. The force switching function [35] was applied to smooth the nonbonded electrostatics and van der Waals potential energy when the internuclear distance for two atoms was between 9 and 12.0 Å. The hydrogen atom-involved covalent bond lengths were constrained by the SHAKE algorithm [36], allowing the use of an integration time step of 2 fs. Prior to production simulations, each system was minimized using a conjugate gradient algorithm to remove the bad contacts of the initial configuration. All simulated systems reached an energy tolerance of 0.0001 kcal/mol after 100,000 minimization steps. A 0.1-ns slow heating simulation was then performed until the system temperature reached 310 K. The trajectories were recorded every 5 ps. Table 1 presents the total simulation time for each simulated system.

All analyses were performed using Pine-MD, an in-house program developed by our group that had been employed in previous MD studies of amyloidogenic peptides [37,38], antimicrobial peptides [39], and lipid bilayers [24]. Several properties were calculated. The populations and structures of the inter-micelle cation–lipid clusters were calculated. When the distance between one cation and a more-electronegative oxygen atom of the lipid (O_{13}, O_{14}, O_{32}, O_{22}, OC_2, or OC_3 atom) was within 3.3 Å, that lipid was considered to be coordinated to the cation [24]. A

Table 1
Names, compositions, and simulation times of the studied systems.

System name	Atoms	POPE	Water	Lipid conc. (M)	W/L[a]	Na^+	Mg^{2+}	Ca^{2+}	Cl^-	Simulation time	Results
Single micelle system											
POPE-Na^+	41382	62	11190	0.31	180.4	31	–	–	31	100 ns	Equilibrium
POPE-Mg^{2+}	41413	62	11190	0.31	180.4	–	31	–	62	100 ns	Equilibrium
POPE-Ca^{2+}	41413	62	11190	0.31	180.4	–	–	31	62	100 ns	Equilibrium
Two Micelles System											
2 M-POPE-Ca^{2+}-SysI	87164	124	23823	0.29	192.1	–	–	65	130	142 ns	Fused
2 M-POPE-Ca^{2+}-SysII	87164	124	23823	0.29	192.1	–	–	65	130	135 ns	Fused
2 M-POPE-Ca^{2+}-SysIII	87164	124	23823	0.29	192.1	–	–	65	130	111 ns	Fused
2 M-POPE-Ca^{2+}-SysIV	87164	124	23823	0.29	192.1	–	–	65	130	100 ns	Unfused
2 M-POPE-Na^+-SysI	87100	124	23824	0.29	192.1	64	–	–	64	250 ns	Unfused
2 M-POPE-Na^+-SysII	87100	124	23824	0.29	192.1	64	–	–	64	100 ns	Unfused
2 M-POPE-Mg^{2+}-SysI	87164	124	23823	0.29	192.1	–	65	–	130	100 ns	Unfused

[a] Water/lipid ratio.

cation coordinated to two more-electronegative oxygen atoms of lipids from a different micelle was considered to be an inter-micelle cation–lipid cluster. The inter-micelle contact number (N_C) was calculated to account for the degree of micelle fusion. Two atoms located on different micelles were considered as one contact when they were separated within a distance of 5 Å. This cutoff was chosen based on the radial distribution function (RDF) of atoms in a single micelle, by which the first peak was covered. The asymmetry parameter (α), calculated to monitor the change in shape of the two micelles during fusion, was defined as [40]

$$\alpha\ (\text{asymmetry parameter}) = \frac{\left(2I_z - I_x - I_y\right)}{\left(I_z - I_x - I_y\right)}$$

where I_x, I_y, and I_z are the moments of inertia in the x, y, and z directions, respectively. The solvent-accessible surface area (SASA) was calculated using the approach described by Lee et al. [41] to measure the degree of exposure of the lipid tails. The lipid tails of POPE were defined as extending from C_{34} to C_{316} in Sn-1 and from C_{24} to C_{218} in Sn-2. These carbon atoms were buried to a greater extent inside the micelle derived from the atom distribution analysis of the simulation of the single micelle (data not shown).

The number of water molecules between two micelles (N_W) was calculated. First, the center of mass (COM) of each micelle was calculated. A vector was calculated from the COM of one micelle to another. The whole system was aligned to the z-axis in space by taking the COM vector of two micelles as the reference; taking the COM of each micelle as the origin, a square was drawn having sides of 40 Å, slightly smaller than the diameter of a micelle (ca. 50 Å). This approach allowed the water molecules in the inter-micellar region to be chosen, but not those located at the surface region of the fusing micelles; a square box was obtained as depicted in Fig. 1. The height of the cylinder, which was equal to the distance between the COMs of two micelles, varied with respect to the simulation time. The water molecules located in the rectangular box were considered as being positioned between the two micelles. The number of water–water hydrogen bonds per water molecule (N_{WW}^{HB}) of the inter-micelle water molecules and water–lipid hydrogen bonds per water molecule were calculated (N_{WL}^{HB}). Hydrogen bonds were calculated using the following criteria [42]: a hydrogen bond between a hydrogen donor (D–H) and a hydrogen acceptor (A) was judged to have formed when the D···A distance was less than 3.3 Å and the angle θ_{HDO} was less than 30.0°, where r_{OO} is the distance between two oxygen atoms and θ_{HDA} is the angle between r_{DA} and the intramolecular D–H bond.

3. Results

To investigate the fusion mechanism, we performed four, two, and one all-atom MD simulations of two-micelle systems with different initial configurations in the presence of Ca^{2+}, Na^+, and Mg^{2+} cations, respectively. For the four MD simulations in the presence of Ca^{2+} ions, we observed spontaneous micelle fusion within a 100-ns simulation for three of the four simulations (an animation is provided in the SI). On the other hand, for the simulations in the presence of either Mg^{2+} or Na^+ cations, we did not observe micelle fusion or stable contact between the two micelles (an animation is provided in the SI); the total simulation times for the Mg^{2+}- and Na^+-containing systems were 100 and 350 ns, respectively.

3.1. Fusion characteristics as a function of time

To understand the characteristics of micelle fusion, we calculated seven parameters of the 2 M-POPE-Ca^{2+} system as a function of the simulation time (Fig. 2): the distance (d_{COM}) between the COMs of two micelles, the inter-micelle contact number (N_C), the asymmetry parameter (α), two types of SASA for the lipid tails, the inter-micelle water number (N_W), and the number of water–water hydrogen bonds per water molecule (N_{WW}^{HB}) of the inter-micelle water molecules. The two different kinds of SASA were (i) the total SASA of the lipid tails of two micelles ($SASA_{tot}$), calculated by taking two micelles into consideration at the same time, and (ii) the sum of the SASA of each micelle's lipid tails ($SASA_{sum}$), where the SASA of each micelle's lipid tails was calculated individually without considering the other micelle. The two micelles in 2 M-POPE-Ca^{2+}-SysIV were not fused until the end of the 100-ns simulation (data not shown). We have marked Fig. 2 with seven vertical lines to indicate the various stages of the fusion process: a red dashed line indicating the initial time when a stable inter-micelle Ca^{2+}–lipid cluster was formed; a green dashed line indicating the initial time of the formation of a pre-stalk state; an orange dashed line indicating the time when a stable stalk state was formed; a black dashed line

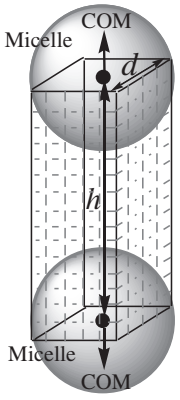

Fig. 1. A graph representing the space located between two micelles. For details, see the text in the computational methods section.

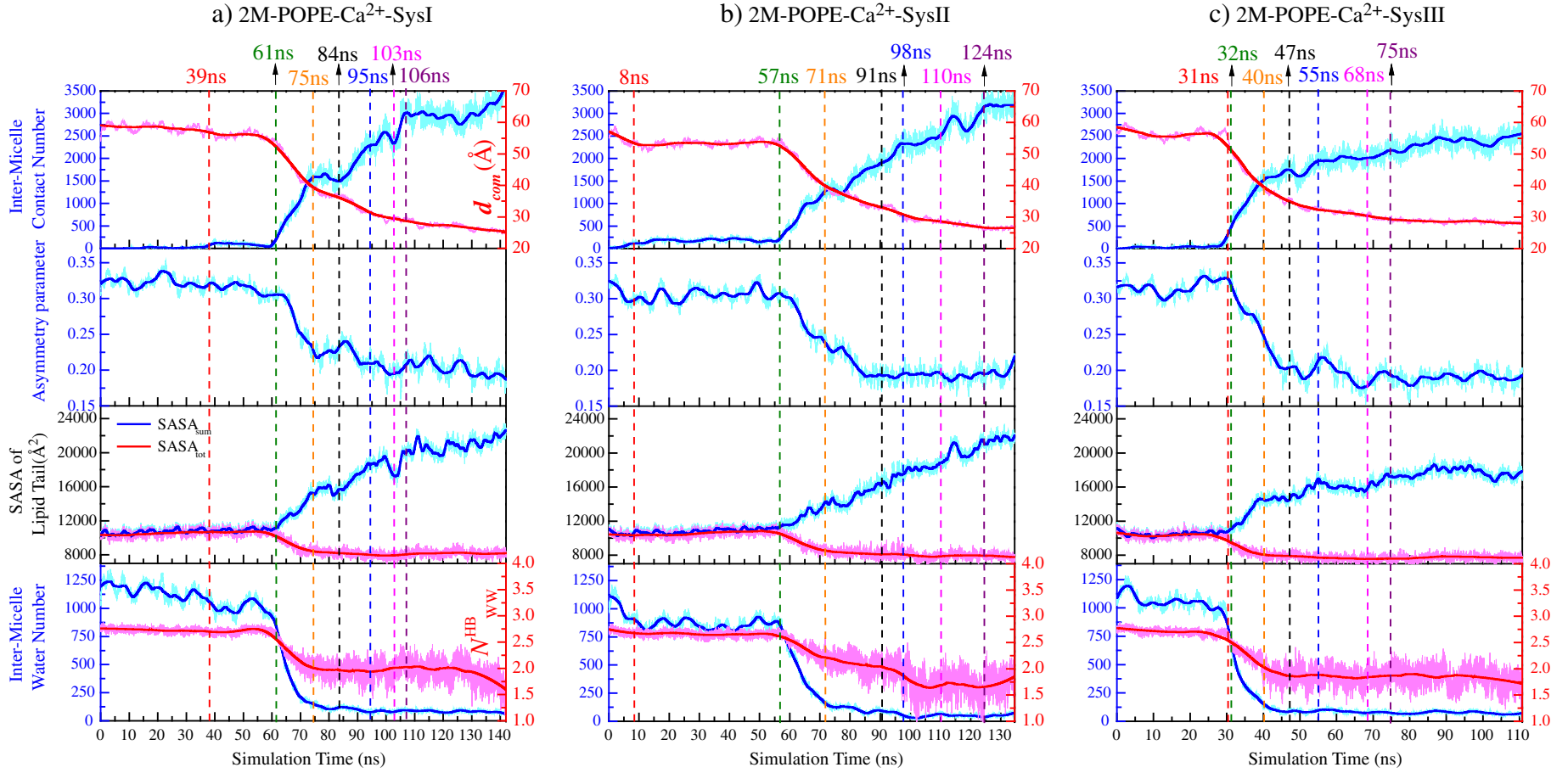

Fig. 2. Seven characteristic properties of micelle fusion of 2 M-POPE-Ca^{2+} systems that evolve over time: distance (d_{COM}) between the COMs of two micelles, inter-micelle contact number (N_C), asymmetry parameter (α), $SASA_{sum}$, $SASA_{tot}$, inter-micelle water number (N_W), the number of water–water hydrogen bonds per water molecule (N_{WW}^{HB}) of the inter-micelle water molecules. For explanations of the vertical lines, see the text.

indicating the initial time of the formation of a hemifused-like state; a blue dashed line indicating the time when a stable hemifused-like state was formed; a magenta dashed line indicating the initial time of the formation of a fused state; and a purple dashed line indicating the time when a stable fused state was formed. These time points and their corresponding states were mainly determined from the trends in the values of N_C and were validated by visualizing the structures of simulated trajectories. 2 M-POPE-Ca^{2+}-SysI is presented in detail as a framework for general fusion events [Fig. 2(a)]. The other 2 M-POPE-Ca^{2+} systems were treated concisely, focusing on their differences from those of 2 M-POPE-Ca^{2+}-SysI.

For 2 M-POPE-Ca^{2+}-SysI, a stable inter-micelle Ca^{2+}–lipid cluster was formed at approximately 39 ns (highlighted by the red dashed line). Thereafter, the value of N_C increased slightly and remained at a similar level until the simulation time reached approximately 61 ns (highlighted by the green dashed line). These results indicate that the inter-micelle Ca^{2+}–lipid clusters bound two micelles together in a stable manner. During the period of time between 31 and 61 ns, the seven calculated structural parameters of 2 M-POPE-Ca^{2+}-SysI [Fig. 2(a)] remained stable. After 61 ns, however, the value of N_C had increased dramatically while the value of d_{COM} had decreased dramatically, revealing the effective fusion of the two micelles. At almost the same time, the asymmetry parameter decreased dramatically, representing the geometric transformation from two separated micelles (more asymmetric) to one fused micelle (more symmetric). We observed the initial formation of the pre-stalk state at approximately 61 ns (highlighted by the green line). The pre-stalk state features lipid tails exposed to the inter-micellar space, as indicated by the increase in the value of $SASA_{sum}$. A stable stalk state was formed at approximately 75 ns (highlighted by the orange dashed line); the stalk state was stable (evidenced by the stable value of N_C) until the simulation time reached approximately 84 ns (highlighted by the black line). A stable hemifused-like state was formed at approximately 95 ns (highlighted by the blue dashed line). The hemifused-like state began transforming into a fused state at approximately 103 ns (highlighted by the magenta dashed line). A stable fused state was formed at approximately 106 ns (highlighted by the purple dashed line). After 61 ns, the value of $SASA_{sum}$ increased dramatically, indicating that the lipids' hydrophobic tails were exposed to the micelle surface region. In contrast, the value of $SASA_{tot}$ decreased slightly, implying that the exposed lipid tails of one micelle were hindered by the other micelle.

After formation of the pre-stalk state, we observed water expulsion from the inter-micellar space, resulting in a dramatic decrease in the

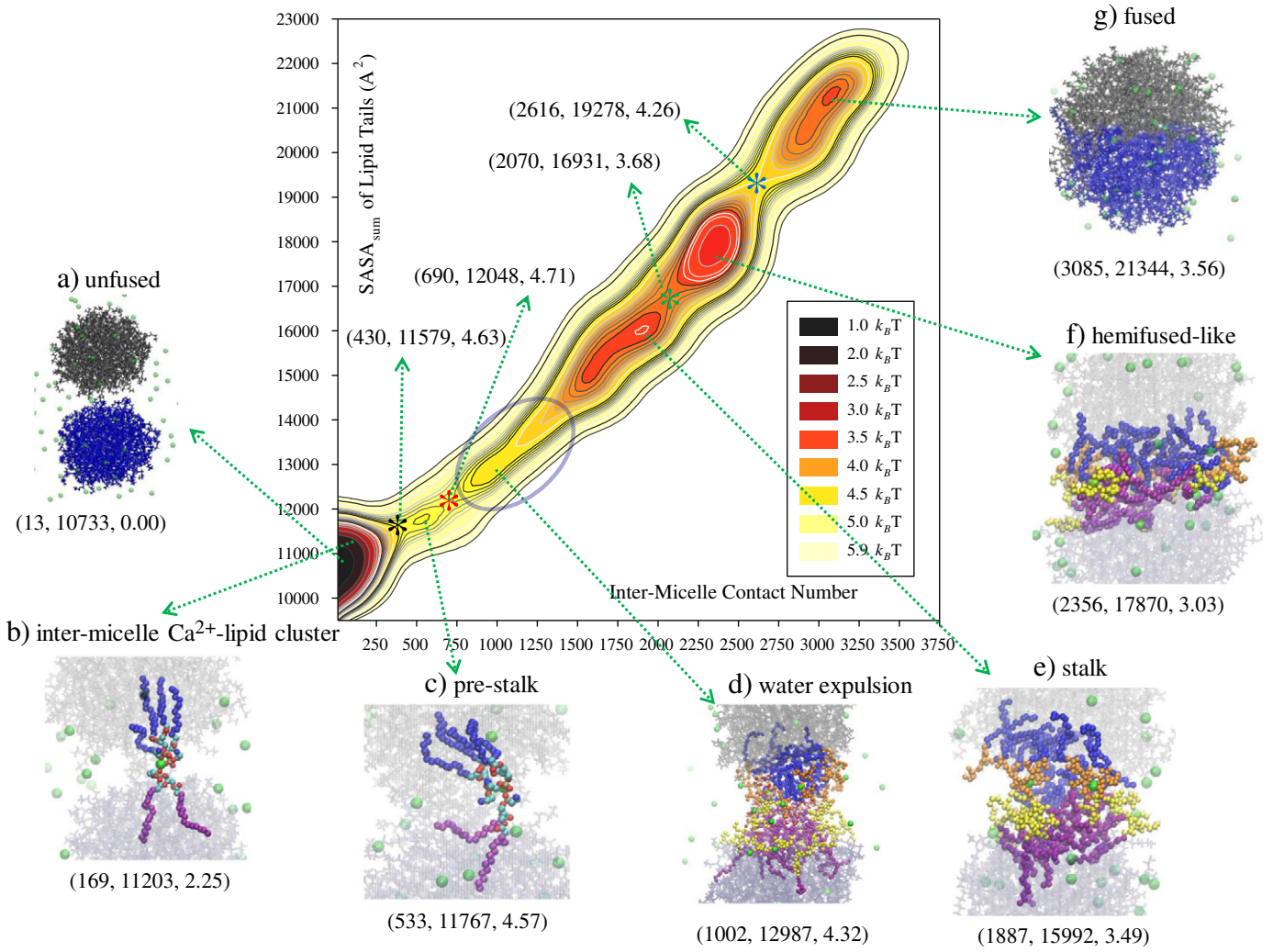

Fig. 3. Free energy landscape of Ca^{2+}-catalyzed micelle fusion at 310 K. The free energy landscape is plotted in terms of the values of N_C and $SASA_{sum}$(Å^2). The three numbers in the parentheses are the values of N_C, $SASA_{sum}$(Å^2), and relative energy, respectively. The units of free energy are given in multiples of k_BT. Representative snapshots of each local minimum and process are provided beside the plot: (a) unfused state; (b) inter-micelle Ca^{2+}–lipid clusters; (c) pre-stalk state; (d) water expulsion process from the inter-micellar space (circled); the relative free energy is for the saddle point; (e) stalk state; (f) hemifused-like state; and (g) fused state. The high-energy saddle points separating two neighboring states are marked by stars.

value of N_W (Fig. 2). Relative to the value of N_W in the initial formation of pre-stalk state, a significant number of water molecules were expelled from the inter-micellar regions when the stable stalk state was formed. The hydrogen bonding pattern of the inter-micelle water molecules was different from that of bulk water, and it changed during the fusion process. Before the water expulsion from the inter-micellar space, we observed that the N_{WW}^{HB} number retained a similar level with $\langle N_{WW}^{HB}\rangle$ of 2.72 and the inter-micelle water molecules form hydrogen bonds with the head groups of lipids with $\langle N_{WL}^{HB}\rangle$ number of 0.11 (Fig. S2); the symbol denotes the average over time and the selected ensembles. The total number of hydrogen bonds of the inter-micelle water molecules was less than that of bulk water (3.14), indicating that the inter-micelle water molecules were oriented with their hydrogen bonding sites facing the lipid's hydrophobic moiety [42,43]. The N_{WW}^{HB} number decreased during the water expulsion process. The $\langle N_{WW}^{HB}\rangle$ number during the simulation time period from 61 to 75 ns was 2.23 and the $\langle N_{WL}^{HB}\rangle$ number (Fig. S2) was 0.17, indicating that 0.43 hydrogen bonds per inter-micelle water molecules were lost during the water expulsion process.

The other two 2 M-POPE-Ca^{2+} systems exhibited similar behavior as discussed above, but different kinetics. For example, the effective fusion process for 2 M-POPE-Ca^{2+}-SysI took approximately 22 ns after the formation of the inter-micelle Ca^{2+}–lipid clusters; 2 M-POPE-Ca^{2+}-SysII took approximately 49 ns; for the 2 M-POPE-Ca^{2+}-SysIII, however, effective fusion occurred immediately after formation of the stable inter-micelle Ca^{2+}–lipid cluster. 2 M-POPE-Ca^{2+}-SysI and 2 M-POPE-Ca^{2+}–SysII required approximately 14 ns to form stable stalk states after the formation of their pre-stalk states; 2 M-POPE-Ca^{2+}-SysIII took approximately 8 ns to complete this process. Furthermore, the formation of the stalk state in 2 M-POPE-Ca^{2+}-SysII was a two-step process: a small stalk state was first formed and was stable during the period 71–78 ns; subsequently, a large stalk state was formed that was stable during the period 85–91 ns. On the other hand, the formation of the stalk states in 2 M-POPE-Ca^{2+}-SysI and 2 M-POPE-Ca^{2+}-SysIII were one-step processes.

3.2. Free energy landscape of Ca^{2+}-catalyzed micelle fusion

To understand the free energy landscape of Ca^{2+}-catalyzed micelle fusion, we projected the trajectories of four 2 M-POPE-Ca^{2+} simulations on two reaction coordinates—the inter-micelle contact number (N_C) and the value of $SASA_{sum}$—in terms of the potential mean force (Fig. 3). We calculated the free energy using the equation

$$\Delta G(q_1, q_2) = -k_B T \ln P(q_1, q_2)$$

where q_1 is the value of N_C, q_2 is the value of $SASA_{sum}$, and $P(q_1,q_2)$ is a canonical probability distribution function; the lowest free energy was set to zero. Fig. 3 reveals the energy basins and saddle points (marked by stars) between two neighboring energy basins. The saddle point is the highest free energy point in the minimum-energy pathway (MEP) connecting two neighboring energy basins. The three numbers in the parentheses below the representative snapshots are the values of N_C, $SASA_{sum}$, and the relative free energy (in multiples of k_BT), respectively. To obtain better ensemble statistics of energy landscape, we calculated the free energy landscape based on four 2 M-POPE-Ca^{2+} simulations. To assess whether the conformational space sampling was sufficient to calculate such an energy landscape, we performed a cross validation procedure using a jack-knifing approach [44]. We randomly removed 5 and 10% of the trajectories at a time and recalculated the free energy landscape. We obtained ten resulting sets of free energy landscapes (nine sets had trajectories removed, one set was the original landscape) and calculated their standard deviations. Fig. S3 (SI) provides the corresponding standard deviations for Fig. 3 with 5 and 10% of trajectories removed. The standard deviations for the low energy regions were generally smaller than those of high energy regions, due to the fact that the high energy region was less sampled [45]. The standard deviations are much smaller than their corresponding energies, indicating that the sampling was sufficient to calculate the energy landscape [46].

The fusion proceeded from the unfused state [Fig. 3(a)] having small values of N_C and $SASA_{sum}$ to the fused state [Fig. 3(g)] having large values of N_C and $SASA_{sum}$. The continued increase in the SASA of the lipid tails on the fusion pathways indicates that reorganization of hydrophobic lipid tails is a significant process during membrane fusion. Fig. 3(b) presents the configuration and relative free energy of the inter-micelle Ca^{2+}–lipid clusters; Fig. 4(a) provides large-scale representations of the configurations of one Ca^{2+} cation bound to one POPE lipid in one micelle and two POPE lipids in another. The hydrophobic tails of the bound lipids were buried within the micelles. The populations of inter-micelle Ca^{2+}–lipid clusters evolved over time (Table S1). The data reveal that the clusters remained stable with more inter-micelle Ca^{2+}–lipid clusters forming during the fusion process.

Fig. 3(c) presents the configuration and relative free energy of the pre-stalk state. The pre-stalk state was a plateau free energy region that was $2.32k_BT$ higher in free energy than that of the inter-micelle Ca^{2+}–lipid cluster state. The activation free energy (E_a) from the inter-micelle Ca^{2+}–lipid cluster state to the pre-stalk state was $2.38k_BT$. Fig. 4(b) displays a large-scale representation of the pre-stalk state with one hydrophobic lipid tail (Sn-2) exposed to the micelle surface and adopting an L shape. Subsequently, the Sn-1 tail of the same lipid was exposed to the micelle surface [Fig. 4(c)]. This lipid with its tails splayed to the micelle surface was participating in the previously formed inter-micelle Ca^{2+}–lipid cluster. We observed that the pre-stalk state had a larger exposed hydrophobic area than did the unfused and inter-micelle Ca^{2+}–lipid cluster states. The pre-stalk states in the three 2 M-POPE-Ca^{2+} simulations with successful fusion had similar features, as mentioned above.

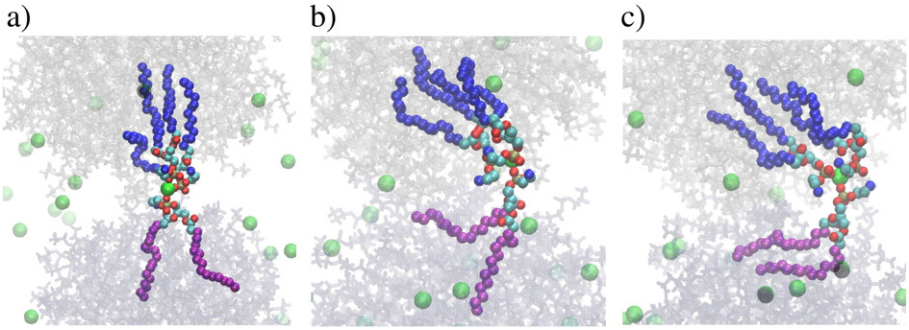

Fig. 4. Representative snapshots of inter-micelle Ca^{2+}–lipid cluster and pre-stalk states. (a) One Ca^{2+} ion binding with one POPE lipid of one micelle and with two POPE lipids of two other micelles; (b) pre-stalk state with one splayed lipid tail; (c) pre-stalk state with two splayed lipid tails. The inter-micelle Ca^{2+}–lipid clusters are highlighted as solid ball-and-stick models, with the hydrophobic tails in different micelles displayed in blue and purple, respectively. Micelles are displayed as transparent line models; Ca^{2+} ions are displayed as green balls.

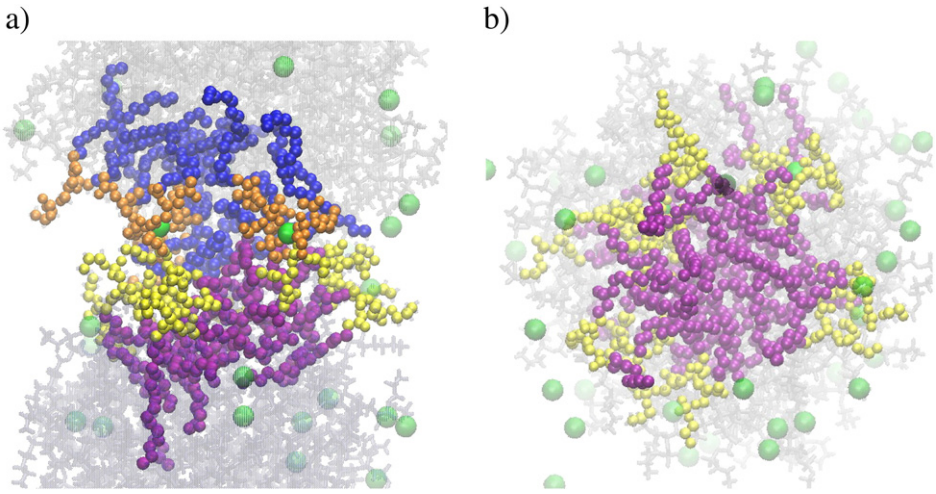

Fig. 5. Representative snapshots of the stalk state. (a) Side-view of the stalk state. The balls colored orange and blue represent the head groups and hydrophobic tails of the lipids, respectively, in the top micelle; the balls colored yellow and purple represent the head groups and hydrophobic tails of the lipids, respectively, in the bottom micelle. (b) Top-view of the stalk state. The balls colored yellow and purple represent the head groups and tails of the lipids, respectively, from two micelles; for clarity, the lipids from different micelles are not distinguished by different colors.

We observed a water expulsion process from the inter-micellar space [circled and a snapshot presented in Fig. 3(d)] after formation of the pre-stalk state [Fig. 3(c)] and prior to formation of the stable stalk state [Fig. 3(e)]. In other words, the water expulsion process occurred in conjunction with the formation of the stalk state. A saddle point (red star in Fig. 3) separating the pre-stalk and stalk states was $0.14k_BT$ higher in free energy than the pre-stalk state. The values of N_C and $SASA_{sum}$ increased upon progressing through the water expulsion process. These results indicate that increasing numbers of lipid tails were exposed from the interior region of the micelle and, at the same time, the lipids from two different micelles were forming more contacts during this process [Fig. 3(d)].

The stalk state [Fig. 3(e)] featured several lipid molecules connecting two micelles, which were interdigitated [Fig. 5(a)]. The stalk state had an hourglass-shaped structure: the hydrophobic lipid tails from each micelle protruded into the inter-micellar region to form a new hydrophobic core [Fig. 5(b)], while the polar head groups of the lipids pointed into the water region. The stalk state was more stable, by a free energy of $1.08k_BT$, than the pre-stalk state.

The free energy of the hemifused-like state [Fig. 3(f)] was comparable with ($0.46k_B$T lower in energy than) that of the stalk state. The value of E_a from the stalk state to the hemifused-like state was $0.19k_B$T. The hemifused-like state featured its inter-micelle structure expanded radially from the stalk state, forming a larger inter-micelle hydrophobic core than that of the stalk state (Fig. 6); consequently, it had a larger value of $SASA_{sum}$ than that of the stalk state. After forming the hemifused-like state, reorganization of the lipids within the two micelles led to their fusion into one large micelle. The value of E_a from the hemifused-like state to the fused state was $1.23k_BT$.

The free energy landscapes of each successful fusion system were calculated separately (Fig. S4). The free energy landscapes of each system featured differences in the locations and relative energies of their energy basins; nevertheless, they had similar fusion features, as discussed above. The most significant difference is that 2 M-POPE-

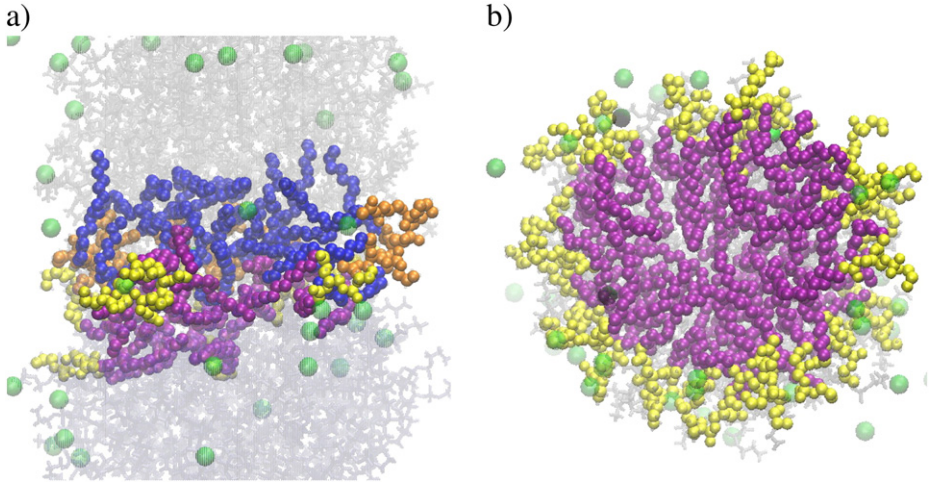

Fig. 6. Representative snapshots of the hemifused-like state. (a) Side-view of the hemifused-like state. The balls colored orange and blue represent the head groups and tails of the lipids, respectively, in the top micelle; the balls colored yellow and purple represent the head groups and tails of the lipids, respectively, in the bottom micelle. (b) Top-view of the hemifused-like state. The balls colored yellow and purple represent the head groups and tails of the lipids, respectively, in two micelles; for clarity, the lipids in different micelles are not distinguished by different colors.

Ca^{2+}-SysII featured two stalk states with hydrophobic cores of different sizes, as discussed in Section 3.1. Taken together, we conclude that formation of the pre-stalk state was the rate-limiting step during the fusion process. The formation of the stalk state was accompanied by a water expulsion process. The neighboring states were separated by an energy barrier.

4. Discussion

The free energies of the membrane fusion intermediates depend on the type of cation present, the type of lipid, the degree of hydration, and the temperature. We have used all-atom MD simulations at 310 K to study the fusion energy landscapes of two POPE micelles with a high degree of hydration in the presence of Ca^{2+} cations, which have been reported to play a critical role in membrane fusion. Previous experiments [22,27] and simulations [23,24] have revealed that Ca^{2+} ions are capable of dehydrating the membrane. Our one-micelle simulations suggested that the presence of Ca^{2+} ions results in more-solvent-exposed lipid tails relative to those obtained in the presence of Na^{+} and Mg^{2+} ions; the calculated SASAs of the lipid tails in our POPE-Ca^{2+}, POPE-Mg^{2+}, and POPE-Na^{+} systems were 5710, 5440, and 5385 $Å^2$, respectively. These results mimic those from in vitro experiments of poly(ethylene glycol) (PEG)-induced fusion of PC vesicles, in which the vesicles are likely to be dehydrated upon the binding of PEG [47]. The more-hydrophobic surface of the POPE-Ca^{2+} micelle ensures that an energetically favorable hydrophobic interaction occurs between two micelles to drive them together. In contrast, our simulations of 2 M-POPE-Na^{+} and 2 M-POPE-Mg^{2+} systems revealed that fusion did not occur—indeed, the two micelles did not even come into close contact.

Our results suggest that the fusion of POPE micelles evolves from the formation of stable inter-micelle Ca^{2+}–lipid clusters. On each micelle, the inter-micelle Ca^{2+}–lipid cluster has at least one Ca^{2+} ion binding with at least one lipid (polar head group), allowing the Ca^{2+} ion to function as a "glue" that holds two micelles together. We observed that the inter-micelle Ca^{2+}–lipid clusters were stable, suggesting that they are capable of binding two micelles together. Earlier studies of lipid bilayers revealed that Ca^{2+} ions are capable of binding two proximal leaflets of lipid bilayers in a "trans" manner and destabilizing the membranes [23,48]. In addition to Ca^{2+} ions, polycations have also been demonstrated, through cryo-TEM and NaCl-leakage experiments, to induce the fusion of anionic liposomes in a conformation-dependent manner [49]. For example, the fusion process is induced by polylysine, but not by the cationic polymer poly(*N*-ethyl-4-vinylpyridinium bromide) (PEVP), presumably because looping and disorganization of the adsorbed PEVP molecules prevent fusion through steric shielding; in contrast, polylysine forms planar β-sheets that are sufficiently thin to allow membrane fusion. The small volume of a Ca^{2+} ion has little steric effect that could retard membrane fusion.

Our free energy landscape for POPE micelle fusion (Fig. 3) suggests that, after the formation of inter-micelle Ca^{2+}–lipid clusters, the fusion event proceeds sequentially through the formation of pre-stalk, stalk, and hemifused-like intermediates, finally providing a fused micelle. The pre-stalk state is $1.08k_BT$ less stable in free energy than the stalk state, consistent with previous findings based on MD simulations in conjunction with a CG model [14]. Moreover, we characterized the formation of the pre-stalk intermediate as the rate-limiting step in the fusion pathway. The pre-stalk state exhibits a plateau free energy region; the pre-stalk intermediate has a loose structure in which one or two lipids adopt an L-shaped conformation with their tails residing on the micelle surface region or partially splayed into the inter-micelle water region. Lipids in the pre-stalk state adopting an L shape have also been observed in previous CG simulations of small vesicles [50] and planar bilayers [14]. Our simulations revealed that an unsaturated Sn-2 chain is always splayed on the micelle surface earlier than a saturated Sn-1 chain, consistent with the results of a previous study [51], presumably because of the degree of packing of an Sn-2 chain within a micelle is lower than that of a saturated Sn-1 chain. Moreover, we observed that the splay of the Sn-2 chain to the micelle surface arose mainly through conformational changes of the C_{29}–C_{210}–C_{211}–C_{212} and/or C_{21}–O_{21}–C_2–C_1 dihedral angles, similar to that reported from a previous MD study [52]. We observed that the splayed lipid in the pre-stalk state was the same lipid involved in the previously formed inter-micelle Ca^{2+}–lipid cluster. As discussed above, the presence of Ca^{2+} ions can lead to an increase in the SASAs of the lipid tails; moreover, a previous study has also revealed that Ca^{2+} ions can destabilize lipid bilayers [23]. Taken together, these results suggest that Ca^{2+} ions can enhance the probability of pre-stalk state formation.

The pre-stalk state with splayed lipid tails diminishes after other lipids aggregate onto it, resulting in an interdigitated lipid bridge with a hydrophobic core stabilizing the structure. This state, with lipids connecting two micelles, is called the stalk state and has been observed in previous studies [14,53,54]. Hydrophobic interactions play important roles in many important biophysical self-assembly processes, including protein folding [55,56], aggregation [57,58], and the formation of micelles and membranes [59].

The energy landscape of membrane fusion depends on many factors, including the type of lipid, the temperature, the surface tension, the types of cations present, and even the models used for the calculations. Our simulations using POPE micelles have captured the essential molecular mechanism of membrane fusion and its free energy landscape. Additional simulations with different initial configurations will improve the accuracy of the calculated free energy landscape of fusion. Simulations using a more-realistic model (e.g., vesicles) may, however, be necessary to provide more information about the membrane fusion process, such as the formation of a hemifused diaphragm. Currently, we are performing fusion simulations using a large vesicle model. This present study provides insight into the molecular mechanisms of micelle and membrane fusion from the points of view of energy, structure, and dynamics.

5. Conclusions and summary

We have used all-atom MD simulations to investigate the free energy landscape of POPE micelle fusion catalyzed by Ca^{2+} ions. Here, we characterized the underlying molecular mechanism of fusion in terms of the free energy landscape with trajectories projected on two structural parameters: the values of N_C and $SASA_{sum}$. We have found that Ca^{2+} ions catalyze the fusion in three aspects: (*i*) they dehydrate the micelle surface and induce the greater exposure of lipid tails, which provide the hydrophobic interactions necessary to attract pairs of micelles; (*ii*) they bind two micelles together to form stable inter-micelle Ca^{2+}–lipid clusters that restrict the motions of the two micelles within a certain distance; and (*iii*) their inter-micelle Ca^{2+}–lipid clusters destabilize the micelle, thereby enhancing the formation of the pre-stalk state. Effective fusion is initiated through the formation of a pre-stalk state featuring lipid tails exposed to the inter-micellar space. The formation of the pre-stalk state is the rate-limiting step. The Ca^{2+} ions play a critical role in catalyzing the formation of the pre-stalk. We observed that stalk state formation occurs in conjunction with a water expulsion process. Our simulations confirm that lipid micelle fusion is affected significantly by the nature of the cation, providing new insight into Ca^{2+}-catalyzed fusion from the points of view of energy, structure, and dynamics.

Acknowledgements

We thank the National Science Council of Taiwan for financial support (grant no.: 100-2113-M-008-003-MY2) and the National Center for High-Performance Computing and the V'ger computer cluster at the National Central University of Taiwan (contribution number: NCU-CCG102-0001) for computer time and facilities.

Appendix A. Supplementary data

Supporting information available: Chemical structure of POPE; inter-micelle water number as a function of time and cutoff distance; atom distribution in a fused micelle; populations of inter-micelle Ca^{2+}–lipid clusters as a function of time; two animations displaying fusion in the 2 M-POPE-Ca^{2+}-SysI system and the absence of contact in the 2 M-POPE-Na^{+}-SysI system. Supplementary data to this article can be found online at http://dx.doi.org/10.1016/j.bbamem.2013.07.022.

References

[1] L.V. Chernomordik, M.M. Kozlov, Membrane hemifusion: crossing a chasm in two leaps, Cell 123 (2005) 375–382.
[2] R. Jahn, T. Lang, T.C. Südhof, Membrane fusion, Cell 112 (2003) 519–533.
[3] J.C. Shillcock, R. Lipowsky, Tension-induced fusion of bilayer membranes and vesicles, Nat. Mater. 4 (2005) 225–228.
[4] P. Kasson, V.S. Pande, Control of membrane fusion mechanism by lipid composition: predictions from ensemble molecular dynamics, PLOS Comput. Biol. 3 (2007) 2228–2238.
[5] A. Portis, C. Newton, W. Pangborn, D. Papahadjopoulos, Studies on the mechanism of membrane fusion: evidence for an intermembrane calcium(2+) ion-phospholipid complex, synergism with magnesium(2+) ion, and inhibition by spectrin, Biochemistry 18 (1979) 780–790.
[6] R. Jahn, H. Grubmüller, Membrane fusion, Curr. Opin. Cell Biol. 14 (2002) 488–495.
[7] L. Yang, H.W. Huang, Observation of a membrane fusion intermediate structure, Science 297 (2002) 1877–1879.
[8] L. Yang, H.W. Huang, A rhombohedral phase of lipid containing a membrane fusion intermediate structure, Biophys. J. 84 (2003) 1808–1817.
[9] S.-J. Marrink, A.E. Mark, Molecular view of hexagonal phase formation in phospholipid membranes, Biophys. J. 87 (2004) 3894–3900.
[10] S.J. Marrink, A.E. Mark, The mechanism of vesicle fusion as revealed by molecular dynamics simulations, J. Am. Chem. Soc. 125 (2003) 11144–11145.
[11] P.M. Kasson, N.W. Kelley, N. Singhal, M. Vrljic, A.T. Brunger, V.S. Pande, Ensemble molecular dynamics yields submillisecond kinetics and intermediates of membrane fusion, Proc. Natl. Acad. Sci. 103 (2006) 11916–11921.
[12] Y. Norizoe, K. Daoulas, M. Muller, Measuring excess free energies of self-assembled membrane structures, Faraday Discuss. 144 (2010) 369–391, (discussion 445-381).
[13] Y. Kozlovsky, M.M. Kozlov, Stalk model of membrane fusion: solution of energy crisis, Biophys. J. 82 (2002) 882–895.
[14] Y.G. Smirnova, S.J. Marrink, R. Lipowsky, V. Knecht, Solvent-exposed tails as prestalk transition states for membrane fusion at low hydration, J. Am. Chem. Soc. 132 (2010) 6710–6718.
[15] A. Grafmuller, J. Shillcock, R. Lipowsky, Pathway of membrane fusion with two tension-dependent energy barriers, Phys. Rev. Lett. 98 (2007) 218101.
[16] D. Mirjanian, A.N. Dickey, J.H. Hoh, T.B. Woolf, M.J. Stevens, Splaying of aliphatic tails plays a central role in barrier crossing during liposome fusion, J. Phys. Chem. B 114 (2010) 11061–11068.
[17] R. Schneggenburger, E. Neher, Presynaptic calcium and control of vesicle fusion, Curr. Opin. Neurobiol. 15 (2005) 266–274.
[18] J. Wilschut, N. Duzgunes, R. Fraley, D. Papahadjopoulos, Studies on the mechanism of membrane fusion: kinetics of calcium ion induced fusion of phosphatidylserine vesicles followed by a new assay for mixing of aqueous vesicle contents, Biochemistry 19 (1980) 6011–6021.
[19] R. Ekerdt, D. Papahadjopoulos, Intermembrane contact affects calcium binding to phospholipid vesicles, Proc. Natl. Acad. Sci. U. S. A. 79 (1982) 2273–2277.
[20] L. Herbette, C.A. Napolitano, R.V. McDaniel, Direct determination of the calcium profile structure for dipalmitoyllecithin multilayers using neutron diffraction, Biophys. J. 46 (1984) 677–685.
[21] C. Altenbach, J. Seelig, Calcium binding to phosphatidylcholine bilayers as studied by deuterium magnetic resonance. Evidence for the formation of a calcium complex with two phospholipid molecules, Biochemistry 23 (1984) 3913–3920.
[22] R. Dluhy, D.G. Cameron, H.H. Mantsch, R. Mendelsohn, Fourier transform infrared spectroscopic studies of the effect of calcium ions on phosphatidylserine, Biochemistry 22 (1983) 6318–6325.
[23] Z.K. Issa, C.W. Manke, B.P. Jena, J.J. Potoff, Ca2+ bridging of apposed phospholipid bilayers, J. Phys. Chem. B 114 (2010) 13249–13254.
[24] H.H. Tsai, W.X. Lai, H.D. Lin, J.B. Lee, W.F. Juang, W.H. Tseng, Molecular dynamics simulation of cation-phospholipid clustering in phospholipid bilayers: possible role in stalk formation during membrane fusion, Biochim. Biophys. Acta 1818 (2012) 2742–2755.
[25] M. Ross, C. Steinem, H.-J. Galla, A. Janshoff, Visualization of chemical and physical properties of calcium-induced domains in DPPC/DPPS Langmuir—Blodgett layers, Langmuir 17 (2001) 2437–2445.
[26] L. Picas, M.T. Montero, A. Morros, M.E. Cabañas, B. Seantier, P.-E. Milhiet, J. Hernández-Borrell, Calcium-induced formation of subdomains in phosphatidylethanolamine—phosphatidylglycerol bilayers: a combined DSC, 31P NMR, and AFM study, J. Phys. Chem. B 113 (2009) 4648–4655.
[27] Z.D. Schultz, I.M. Pazos, F.K. McNeil-Watson, E.N. Lewis, I.W. Levin, Magnesium-induced lipid bilayer microdomain reorganizations: implications for membrane fusion, J. Phys. Chem. B 113 (2009) 9932–9941.
[28] Z.D. Schultz, I.W. Levin, Lipid microdomain formation: characterization by infrared spectroscopy and ultrasonic velocimetry, Biophys. J. 94 (2008) 3104–3114.
[29] H. Binder, O. Zschörnig, The effect of metal cations on the phase behavior and hydration characteristics of phospholipid membranes, Chem. Phys. Lipids 115 (2002) 39–61.
[30] V. Knecht, S.-J. Marrink, Molecular dynamics simulations of lipid vesicle fusion in atomic detail, Biophys. J. 92 (2007) 4254–4261.
[31] J.B. Klauda, R.M. Venable, J.A. Freites, J.W. O'Connor, D.J. Tobias, C. Mondragon-Ramirez, I. Vorobyov, A.D. MacKerell, R.W. Pastor, Update of the CHARMM all-atom additive force field for lipids: validation on six lipid types, J. Phys. Chem. B 114 (2010) 7830–7843.
[32] W.L. Jorgensen, J. Chandrasekhar, J.D. Madura, R.W. Impey, M.L. Klein, Comparison of simple potential functions for simulating liquid water, J. Chem. Phys. 79 (1983) 926–935.
[33] L. Kale, R. Skeel, M. Bhandarkar, R. Brunner, A. Gursoy, N. Krawetz, J. Phillips, A. Shinozaki, K. Varadarajan, K. Schulten, NAMD2: greater scalability for parallel molecular dynamics, J. Comp. Phys. 151 (1999) 283–312.
[34] S.E. Feller, Y.H. Zhang, R.W. Pastor, B.R. Brooks, Constant-pressure molecular-dynamics simulation — the Langevin piston method, J. Chem. Phys. 103 (1995) 4613–4621.
[35] P.J. Steinbach, B.R. Brooks, New spherical-cutoff methods for long-range forces in macromolecular simulation, J. Comput. Chem. 15 (1994) 667–683.
[36] J.-P. Ryckaert, G. Ciccotti, H.J.C. Berendsen, Numerical integration of the Cartesian equations of motion of a system with constraints: molecular dynamics of n-alkanes, J. Comp. Phys. 23 (1977) 327–341.
[37] H.-H.G. Tsai, J.-B. Lee, S.-S. Tseng, X.-A. Pan, Y.-C. Shih, Folding and membrane insertion of amyloid-beta (25–35) peptide and its mutants: implications for aggregation and neurotoxicity, Proteins: Struct. Funct. Bioinf. 78 (2010) 1909–1925.
[38] H.H. Tsai, M. Reches, C.J. Tsai, K. Gunasekaran, E. Gazit, R. Nussinov, Energy landscape of amyloidogenic peptide oligomerization by parallel-tempering molecular dynamics simulation: significant role of Asn ladder, Proc. Natl. Acad. Sci. U. S. A. 102 (2005) 8174–8179.
[39] C.-W. Tsai, N.-Y. Hsu, C.-H. Wang, C.-Y. Lu, Y. Chang, H.-H.G. Tsai, R.-C. Ruaan, Coupling molecular dynamics simulations with experiments for the rational design of indolicidin-analogous antimicrobial peptides, J. Mol. Biol. 392 (2009) 837–854.
[40] D.P. Tieleman, D. van der Spoel, H.J.C. Berendsen, Molecular dynamics simulations of dodecylphosphocholine micelles at three different aggregate sizes: micellar structure and chain relaxation, J. Phys. Chem. B 104 (2000) 6380–6388.
[41] B. Lee, F.M. Richards, The interpretation of protein structures: estimation of static accessibility, J. Mol. Biol. 55 (1971) 379-IN374.
[42] N. Galamba, Water's structure around hydrophobic solutes and the iceberg model, J. Phys. Chem. B 117 (2013) 2153–2159.
[43] T.M. Raschke, M. Levitt, Nonpolar solutes enhance water structure within hydration shells while reducing interactions between them, Proc. Natl. Acad. Sci. U. S. A. 102 (2005) 6777–6782.
[44] B.A. Joughin, M.B. Yaffe, B. Tidor, Computational prediction of protein phosphopeptide-binding sites, Protein Sci. 13 (2004) 131–139.
[45] For examples, the high-energy saddle points shown in Fig. 3 were sampled 12–35 times and the higher energy pre-stalk state was sampled 14 times, which are smaller than those of 42 and 67 times for the low-energy stalk and hemifused-like states. We note the sampled times shown here are the times when the representative pixels (indicating the energies of corresponding states) in Fig. 3 was sampled.
[46] For clarity, we summarized the average standard deviations for an energy interval of 0.5 k_BT. For the set with 5% of trajectories removed, the average standard deviations are 0.009, 0.009, 0.012, 0.015, 0.018, 0.025, 0.030, 0.039, 0.048, 0.063, 0.081 and 0.106 k_BT for the free energies in the range of 0–0.5, 0.5–1.0, 1.0–1.5, 1.5–2.0, 2.0–2.5, 2.5–3.0, 3.0–3.5, 3.5–4.0, 4.0–4.5, 4.5–5.0, 5.0–5.5 and 5.5–6.0 k_BT, respectively. For the set with 10% of trajectories removed, the average standard deviations are 0.011, 0.013, 0.018, 0.023, 0.027, 0.034, 0.045, 0.056, 0.070, 0.092, 0.121 and 0.163 k_BT for the free energies in the range of 0–0.5, 0.5–1.0, 1.0–1.5, 1.5–2.0, 2.0–2.5, 2.5–3.0, 3.0–3.5, 3.5–4.0, 4.0–4.5, 4.5–5.0, 5.0–5.5 and 5.5–6.0 k_BT, respectively.
[47] R.I. MacDonald, Membrane fusion due to dehydration by polyethylene glycol, dextran, or sucrose, Biochemistry 24 (1985) 4058–4066.
[48] J.J. Potoff, Z. Issa, C.W. Manke, B.P. Jena, Ca^{2+}-dimethylphosphate complex formation: providing insight into Ca^{2+}-mediated local dehydration and membrane fusion in cells, Cell Biol. Int. 32 (2008) 361–366.
[49] A.A. Yaroslavov, A.V. Sybachin, E. Kesselman, J. Schmidt, Y. Talmon, S.A.A. Rizvi, F.M. Menger, Liposome fusion rates depend upon the conformation of polycation catalysts, J. Am. Chem. Soc. 133 (2011) 2881–2883.
[50] A.F. Smeijers, A.J. Markvoort, K. Pieterse, P.A.J. Hilbers, A detailed look at vesicle fusion, J. Phys. Chem. B 110 (2006) 13212–13219.
[51] P.K. Kinnunen, Fusion of lipid bilayers: a model involving mechanistic connection to HII phase forming lipids, Chem. Phys. Lipids 63 (1992) 251–258.
[52] S. Ohta-Iino, M. Pasenkiewicz-Gierula, Y. Takaoka, H. Miyagawa, K. Kitamura, A. Kusumi, Fast lipid disorientation at the onset of membrane fusion revealed by molecular dynamics simulations, Biophys. J. 81 (2001) 217–224.
[53] S.J. Marrink, A.E. Mark, Molecular dynamics simulation of the formation, structure, and dynamics of small phospholipid vesicles, J. Am. Chem. Soc. 125 (2003) 15233–15242.

[54] V. Knecht, A.E. Mark, S.-J. Marrink, Phase behavior of a phospholipid/fatty acid/water mixture studied in atomic detail, J. Am. Chem. Soc. 128 (2006) 2030–2034.
[55] X. Huang, C.J. Margulis, B.J. Berne, Dewetting-induced collapse of hydrophobic particles, Proc. Natl. Acad. Sci. U. S. A. 100 (2003) 11953–11958.
[56] R.D. Mountain, D. Thirumalai, Molecular dynamics simulations of end-to-end contact formation in hydrocarbon chains in water and aqueous urea solution, J. Am. Chem. Soc. 125 (2003) 1950–1957.
[57] Z. Yang, B. Shi, H. Lu, P. Xiu, R. Zhou, Dewetting transitions in the self-assembly of two amyloidogenic β-sheets and the importance of matching surfaces, J. Phys. Chem. B 115 (2011) 11137–11144.
[58] M.G. Krone, L. Hua, P. Soto, R. Zhou, B.J. Berne, J.-E. Shea, Role of water in mediating the assembly of Alzheimer amyloid-β Aβ16−22 protofilaments, J. Am. Chem. Soc. 130 (2008) 11066–11072.
[59] G. Hummer, S. Garde, A.E. Garcia, L.R. Pratt, New perspectives on hydrophobic effects, Chem. Phys. 258 (2000) 349–370.